

Study of time evolution of the bend-over energy in the energetic particle spectrum at a parallel shock

F.-J. KONG,¹ G. QIN,¹ S.-S. WU,¹ L.-H. ZHANG,² H.-N. WANG,² T. CHEN,³ AND P. SUN⁴

¹*School of Science, Harbin Institute of Technology, Shenzhen, 518055, China; qingang@hit.edu.cn*

²*Key Laboratory of Solar Activity, National Astronomical Observatories, Chinese Academy of Sciences, Beijing, 100012, China*

³*State Key Laboratory of Space Weather, National Space Science Center, Chinese Academy of Sciences, Beijing, 100190, China*

⁴*Department of Planetary Sciences and Astronomy, University of Arizona, Tucson, AZ 85721, USA*

ABSTRACT

Shock acceleration is considered one of the most important mechanisms for the acceleration of astrophysical energetic particles. In this work, we calculate the trajectories of a large number of test charged particles accurately in a parallel shock with magnetic turbulence. We investigate the time evolution of the accelerated-particle energy spectrum in the downstream of the shock in order to understand the acceleration mechanism of energetic particles. **From simulation results we obtain power-law energy spectra with a bend-over energy, E_0 , increasing with time.** With the particle mean acceleration time and mean momentum change during each cycle of the shock crossing from diffusive shock acceleration model (following Drury), a time-dependent differential equation for the maximum energy, E_{acc} , of particles accelerated at the shock, can be approximately obtained. We assume the theoretical bend-over energy as E_{acc} . It is found that the bend-over energy from simulations agrees well with the theoretical bend-over energy using the non-linear diffusion theory, NLGCE-F, in contrast to that using the classic quasi-linear theory (QLT).

Keywords: acceleration of particles–shock waves–magnetic turbulence–energy spectrum–
bend-over energy

1. INTRODUCTION

The collisionless shock acceleration of energetic particles, which is considered to be one of the key problems to study the sources of solar energetic particles (SEPs) and galactic cosmic rays (GCRs), has been studied by many scholars in decades (e.g., Fermi 1949; Bell 1978; Jokipii 1982; Drury 1983; Decker 1988; Krüls and Achterberg 1994; Lee et al. 1996; Zank et al. 2000; Bell 2004; Sun et al. 2007; Florinski et al. 2008; Li et al. 2012; Wang et al. 2012; Qin et al. 2013, 2018; Zuo et al. 2013; Qi et al. 2017; Kong et al. 2017). Different physical mechanisms have been developed to explain the shock acceleration processes. One mechanism is shock drift acceleration (SDA) (Jokipii 1982; Forman and Webb 1985; Lee et al. 1996; Shapiro and Üçer 2003; Guo et al. 2014), **which mainly occurs at perpendicular or quasi-perpendicular shocks. The discontinuous tangential component of the magnetic field across the shock results in the gradient drift of the particles along the shock front in the direction as the electric field in the shock frame.** In this case, the energy gain for each gyro-cycle, ΔE , can be shown in the form of

$$\Delta E = qE \cdot \Delta x, \quad (1)$$

where Δx is the particle displacement variance, and the drift electrostatic field in the shock frame, E , is given by

$$E = -U \times B, \quad (2)$$

where U is the background bulk velocity. **Note that if particles have initial speeds that are comparable to the background flow speed, they would move along the magnetic field lines and convect into the downstream. The SDA therefore generally has an injection problem for low-energy particles (e.g., Ellison et al. 1995; Jokipii & Giacalone 1996).** However, low-energy particles can cross the shock repeatedly under large-scale magnetic fluctuations, and are effectively injected into diffusive shock acceleration (Giacalone 2005a,b).

Another mechanism is first-order Fermi acceleration, which, together with SDA, is incorporated into the diffusive shock acceleration (DSA) (Fermi 1949; Bell 1978; Drury 1983; Forman and Webb 1985; Kirk and Schneider 1987; Malkov and Drury 2001; Amato and Blasi 2005, 2006). In the first-order Fermi acceleration mechanism, the acceleration of particles is derived from the relative motion of the scattering centers in the upstream and downstream of the shock. Drury (1983) showed that for each cycle of the particle's crossing of the shock front, the mean acceleration time Δt is

$$\Delta t = \frac{4}{v} \left(\frac{\kappa_1}{U_1} + \frac{\kappa_2}{U_2} \right), \quad (3)$$

and the average momentum change is

$$\begin{aligned} \langle \Delta p \rangle &= 2p \int_0^1 \frac{\mu(U_1 - U_2)}{v} 2\mu d\mu \\ &= \frac{4}{3} \frac{U_1 - U_2}{v} p, \end{aligned} \quad (4)$$

where κ and U represent the diffusion coefficient and background bulk velocity, respectively, the subscripts 1 and 2 indicate variables in the upstream and downstream, respectively, and μ is the particle's pitch angle cosine. Note that 2μ in the first line of Equation (4) is the statistical weighting factor. If there is non-zero background magnetic field parallel to the shock normal, a particle gains energy during its reflection between the upstream and downstream regions because of diffusion parallel to the background magnetic field. Generally, **first-order Fermi acceleration mechanism** is not considered to have the injection problem. It is shown that with DSA the slope of the energy spectrum, γ , satisfies (Decker and Vlahos 1986)

$$\gamma = \frac{r + 2}{2(r - 1)}, \quad (5)$$

where r is the compression ratio across the shock.

The third mechanism is stochastic acceleration (SA) associated with the magnetic turbulence, also referred to as second-order Fermi acceleration (Krüells and Achterberg 1994; Virtanen and Vainio 2005). The driving force of the SA process is the stochastic electric field $E_b = -U \times \delta \mathbf{b}$, where $\delta \mathbf{b}$ is the turbulent magnetic field superimposed on the mean magnetic field \mathbf{B} .

With the great development of supercomputers' computational capabilities, various numerical simulation methods are proposed to better understand the acceleration processes of particles. The transport and accel-

eration of energetic particles in the heliosphere can be generally studied by analyzing particle trajectories which are obtained by solving the equation of motion of particles in electromagnetic (EM) fields. If the EM fields are assumed to model a shock, the particle trajectory approach can be used to study the shock acceleration (e.g., [Decker and Vlahos 1986](#)). This method of numerical simulations usually requires large computational cost and is limited to available resources, but if one is not interested in individual particle movements especially the details of particle gyromotions, the Fokker-Planck transport equation of energetic particles can be applied to describe the change of the distribution function ([Parker 1965](#); [Skilling 1971](#); [Qin et al. 2004, 2006](#)). [Zuo et al. \(2011, 2013\)](#) used a computational effective method based on the transport equation to study the shock acceleration of energetic particles. However, with this method one has to assume the model of particle diffusion that is not always established in reality.

Charged particles can be accelerated by a shock, and in turn, shock-accelerated particles would influence EM fields or even excite shock waves. Therefore, the particle acceleration and EM fields evolution have to be coupled. Hybrid simulations are a particle-in-cell-type model that treats electrons as a massless fluid while treats ions kinetically ([Winske and Omid 1996](#)). In kinetic simulations Maxwell's equations are solved self-consistently based upon plasma density and currents, which themselves are generated from plasma particles ([Winske and Omid 1996](#)). Under certain conditions hybrid codes can be used to study particle acceleration and shock evolution self-consistently (e.g., [Giacalone 2004, 2005b](#); [Guo and Giacalone 2010](#); [Sugiyama 2011](#)). Hybrid codes, however, are more complicated requiring massive prior programming and extensive computational resources. In order to pay more attention to the shock acceleration of energetic particles in some specific shock conditions (e.g., geometry, compression ratio, magnetic fields, shock speed, and magnetic turbulence model), with more statistics but less resources needed, the test particle model that does not include the feedback of energetic particles to the EM fields, can be very useful.

The diffusion of energetic particles in magnetic turbulence is very important to study shock acceleration of energetic particles. [Jokipii \(1966\)](#) developed a classical quasi-linear theory (QLT) of energetic particles diffusion in a slab model of magnetic turbulence. [Matthaeus et al. \(2003\)](#) introduced the NonLinear Guiding Center (NLGC) theory for the perpendicular diffusion coefficient. [Qin \(2007\)](#) modified the NLGC theory for perpendicular diffusion to obtain a NonLinear PARallel (NLPA) diffusion theory. It was shown that

the solution of the NLGC and NLPA simultaneously agreed with simulations very well. Furthermore, [Qin and Zhang \(2014\)](#) obtained a NLGCE-F model by fitting the numerical results of the NLGC+NLPA model with polynomials. Using the model NLGCE-F one can calculate the parallel and perpendicular diffusion coefficients with much reduced calculations.

Due to the effects of adiabatic deceleration, limited particle acceleration time, and shock geometries, the energy spectrum of energetic particles in SEP events usually shows a power law with a rollover at high energies (e.g., exponential tail) ([Ellison and Ramaty 1985](#))

$$\frac{dJ}{dE} = CE^{-\alpha} \exp\left(-\frac{E}{E_0}\right), \quad (6)$$

where C is a constant, α is the spectral index, and E_0 is the bend-over energy.

In the present paper, we study the parallel shock acceleration of test particles by numerically solving the equation of motion of particles in the shock frame in prescribed turbulent magnetic field. By calculating the trajectories of a large number of particles we obtain power-law energy spectra of accelerated particles with a bend-over energy E_0 . We then investigate the variation of E_0 over time and compare the simulations with the results from theoretical models. We describe our simulation model in section 2, followed by the theoretical models of the bend-over energy in section 3. In section 4, we present the numerical results and the comparison with different models. Finally, we show conclusions and discussions in section 5.

2. SIMULATION MODELS

The test-particle trajectory in the shock frame is controlled by the equation of motion

$$\frac{d\mathbf{p}}{dt} = q(\mathbf{E} + \mathbf{v} \times \mathbf{B}), \quad (7)$$

where \mathbf{p} , \mathbf{v} , and q are the particle momentum, velocity, and electric charge, respectively, and \mathbf{E} and \mathbf{B} are the local electric field and magnetic field, respectively. We simplify the shock as an infinite plane ([Kong et al. 2017](#); [Qin et al. 2018](#)). The shock normal is in the direction anti-parallel to the z axis, and the shock lies in the $x - y$ plane. The upstream and downstream plasma speed, U_1 and U_2 , are both assumed to be parallel to the shock normal. The average magnetic fields in the upstream and downstream regions, are \mathbf{B}_{01} and \mathbf{B}_{02} , respectively.

We use a composite slab plus two-dimensional (2-D) model of static turbulent magnetic field (Matthaeus et al. 1990; Mace et al. 2000; Qin et al. 2002a,b), which is different from that in Decker and Vlahos (1986). The total magnetic field is written as

$$\mathbf{B}(x', y', z') = \mathbf{B}_0(z') + \mathbf{b}(x', y', z'), \quad (8)$$

where a Cartesian coordinate system is adopted, and the z' -axis is in the direction parallel to the mean magnetic field \mathbf{B}_0 . The turbulent magnetic fluctuations, \mathbf{b} , are composed of a slab and 2D component,

$$\mathbf{b}(x', y', z') = \mathbf{b}_{slab}(z') + \mathbf{b}_{2D}(x', y'), \quad (9)$$

where both of the two components are perpendicular to \mathbf{B}_0 .

The induced electric field $|e_k| \approx V_A |\mathbf{b}_k|$ of the turbulent magnetic field $\mathbf{b}_k(z)$ in the plasma frame is neglected because of the fact that the Alfvén speed is far lower than the speed of particles ($V_A \ll |\mathbf{v}|$) (Jokipii 1971; Decker and Vlahos 1986). Therefore, there is no electric field in the plasma frame on each side of the shock plane, and in the shock frame of reference the electric field \mathbf{E} is from the convection due to the plasma bulk speed. In our simulations, the turbulence has a Kolmogorov's spectrum with a power index of $\nu = -5/3$ at the high wavenumber k for each component. Except the shock compression ratio $r = 3.85$, the other background parameters are chosen as those in Decker and Vlahos (1986). In the upstream, the mean magnetic field is $B_{01} = 50$ G, the Alfvén speed is $V_{A1} = 1.1 \times 10^6$ m/s, and the bulk velocity is $U_1 = 3.3 \times 10^6$ m/s. The correlation length of the slab component of the turbulent magnetic field is $\lambda = 6.67 \times 10^{-9}$ au = 1.00×10^3 m. The turbulent magnetic field $\mathbf{b}_{slab}(z')$ is created with fast Fourier transform (FFT) in a box with a size $L_{z'} = 64\lambda$ along the mean magnetic field \mathbf{B}_0 and number of grids $N_{z'} = 2^{22} = 4194304$. In addition, to be different from that in Decker and Vlahos (1986), we apply the 2D component magnetic turbulence with the 2D correlation scale $\lambda_x = \lambda/2.6$ (Osman & Horbury 2007; Dosch et al. 2013; Weygand et al. 2009, 2011; Shen & Qin 2018), in a box with a size $L_{x'} = L_{y'} = 10\lambda$ and number of grids $N_{x'} = N_{y'} = 4096$. The energy ratio of the two components of turbulence is taken to be $E_{slab} : E_{2D} = 1 : 4$. The turbulent level, $(b/B_0)^2$, is set 0.19 and 0.38 in the up- and down-stream, respectively. In the downstream side, the bulk velocity U_2 and mean magnetic field \mathbf{B}_{02} are obtained from the Rankine-Hugoniot relations. Since the average of turbulence magnetic field is zero and turbulence

level is small, we do not consider the Rankine-Hugoniot relations for the turbulent magnetic field in the downstream of the shock.

We adopt a numerical code developed by Sun et al. (2007) (also used in Kong et al. (2017) and Qin et al. (2018)) using an adjustable time step fourth-order Runge-Kutta method with an accuracy of 10^{-9} to obtain test particle trajectories by solving the equation of motion of particles, Equation (7). A total of 60,000 protons with an initial energy of $E_{in} = 30$ keV in the shock frame are isotropically injected in the upstream with a distance $d = 1.1r_g$ to the shock front, where r_g is the proton gyroradius. **The simulations of test particles are performed with an longest acceleration time of $t_{acc} = 500$ ms without space limitations.**

3. THEORETICAL MODELS

3.1. Models of Diffusion

On the basis of the nonlinear diffusion theory (Qin and Zhang 2014, NLGCE-F), we can calculate κ_{\parallel} using the computer code downloaded from the website <http://www.qingang.org.cn/code/NLGCE-F> for different proton momentum in both up- and down-stream. Besides, using quasi-linear theory (QLT) (Jokipii 1966), we have (see also, e.g., Qin 2002)

$$\kappa_{\parallel} = 1.72 \frac{\lambda^{2/3} B_0^{-1/3}}{(b_{slab}/B_0)^2} \left(\frac{R}{c}\right)^{1/3} v, \quad (10)$$

considering the spectral index of slab turbulence in the inertial range being $5/3$. According to QLT with Equation (10), it can be assumed that diffusion coefficients κ can be written as

$$\kappa = \kappa_R \left(\frac{p}{p_{ref}}\right)^{\xi}, \quad (11)$$

where κ_R and ξ are constants, and $p_{ref} = 5.34 \times 10^{-19}$ kg · m/s is the momentum of a proton with rigidity $R = 1$ GV.

Figure 1 shows parallel diffusion coefficients, κ_{\parallel} as a function of particle momentum p/p_{ref} , where p_{ref} is the momentum of a proton with rigidity $R = 1$ GV. Here we show variables in up- and down-stream with subscripts $i = 1$ and 2 , color black and red, respectively. The diamonds represent calculation results from NLGCE-F. The solid lines indicate the fitting of the NLGCE-F results using the power-law form in Equation (11) with parameters ξ_i and κ_{Ri} . To replace the power indice ξ_1 and ξ_2

with the average value, $(\xi_1 + \xi_2)/2$, the solid lines are changed to the dashed ones. It is shown that the dashed lines agree approximately with the solid ones, so one can adopt the average value ξ for both up- and down-stream in NLGCE-F. In addition, the dotted lines indicate the QLT results with parameters ξ_i and κ_{Ri} in Equation (11) obtained from the formula (10) analytically. Here for QLT, $\xi = \xi_1 = \xi_2$. The values of ξ_i and κ_{Ri} from NLGCE-F and QLT are listed in Table 1.

3.2. Model of The Bend-Over Energy

It is very interesting to study the time evolution of the bend-over energy if we assume SEPs are accelerated by a shock. Using the DSA model (Drury 1983) for each shock crossing of particles, from Equation (3) and Equation (4), one can obtain

$$\frac{dp}{dt} \approx \frac{\Delta p}{\Delta t} = \frac{1}{3} (U_1 - U_2) \left(\frac{\kappa_1}{U_1} + \frac{\kappa_2}{U_2} \right)^{-1} p. \quad (12)$$

As seen from Equation (12), the acceleration rate of particles by the shock depends on the diffusion coefficient κ_i , which allows us to get different models of shock acceleration rate with different diffusion models.

The momentum, p_{acc} , of accelerated particles is obtained by integrating Equation (12) considering Equation (11),

$$\left(\frac{p_{acc}}{p_{ref}} \right)^{\xi_1} + g \left(\frac{p_{acc}}{p_{ref}} \right)^{\xi_2} = \left(\frac{p_0}{p_{ref}} \right)^{\xi_1} + g \left(\frac{p_0}{p_{ref}} \right)^{\xi_2} + \frac{1}{3} \frac{U_1^2}{r\kappa_{R1}} \xi_1 (r-1)t, \quad (13)$$

where $g = \xi_1 \kappa_{R2} r / (\xi_2 \kappa_{R1})$, p_0 is the particle initial momentum, and the corresponding energy E_{acc} is

$$E_{acc} = \sqrt{p_{acc}^2 c^2 + E_p^2} - E_p, \quad (14)$$

where E_p is the static energy of a proton. The Equation (13) is an implicit, by numerically solving which the particle momentum p_{acc} with time t of shock acceleration could be obtained. It is less possible for particles to be accelerated to energies higher than E_{acc} . Therefore, the energy spectrum of particles accelerated by a shock would turn over at the energy above E_{acc} , and we can define a bend-over energy, E_0 , as a function of time t

$$E_0 \equiv E_{acc} = \sqrt{p_{acc}^2 c^2 + E_p^2} - E_p. \quad (15)$$

If $\xi_1 = \xi_2 \equiv \xi$, the Equation (13) could be solved directly as,

$$p_{acc} = p_{ref} \left[\left(\frac{p_0}{p_{ref}} \right)^\xi + \frac{U_1^2 \xi}{3} \frac{r-1}{r(\kappa_{R1} + r\kappa_{R2})} t \right]^{1/\xi}. \quad (16)$$

Since we study parallel shock acceleration in this work, diffusion coefficients κ_1 and κ_2 in Equation (12) refer to parallel diffusion. Note that for QLT, we can directly get p_{acc} from Equation (16) due to the fact that the power indice in the up- and down-stream are the same. Whereas for NLGCE-F, ξ_1 in the upstream is not equal to ξ_2 in the downstream. In order to get an explicit expression of particle momentum p_{acc} in Equation (13), we assume ξ as $(\xi_1 + \xi_2)/2$. Therefore, the momentum of accelerated particles p_{acc} with QLT and NLGCE-F can be calculated directly from Equation (16), and the corresponding bend-over energy, which are indicated by E_0^{QLT} and $E_0^{NLGCE-F}$, respectively, could be obtained.

3.3. Energy Spectrum Power Law Index

As discussed in Decker and Vlahos (1986), if charged particles are injected near the shock and accelerated for a time long enough, the energy spectrum becomes stable with a power law index γ satisfying Equation (5). In this work, the compression ratio of the shock is $r = 3.85$, so the energy spectrum of the accelerated particles, has a theoretical power law index of $\gamma = 1.03$. The spectral index from simulations, α , in Equation (6) in the energy range below the bend-over energy, can be compared with the theoretical power law index γ .

4. NUMERICAL RESULTS AND COMPARISON WITH THEORIES

Figure 2 illustrates the trajectory of one of the test particles accelerated by a parallel shock as a function of time. The top three panels show the x -, y -, and z - components, respectively, of the particle position in units of λ . The fourth to sixth panels show the x -, y -, and z - components, respectively, of the particle momentum in units of p_{ref} . The bottom panel shows the particle energy in units of its initial energy $E_0 = 30$ keV. Generally, a particle will get accelerated and gain energy when it crosses the shock plane back and forth. From the top three panels of Figure 2 we can see that within the initial ~ 0.06 s (vertical dashed line), the particle crosses the shock plane many times, but beyond ~ 0.06 s the particle does not cross the shock any more, as the z - component of particle position increases persistently with time, indicating the particle moves far away from the shock plane. In addition, from the 4th to 6th panels of Figure 2, one can find that the particle generally performs gyro-rotation in the $x - y$ plane. It can be seen that within ~ 0.06 s the crests of p_x and p_y increase much more significantly than the crests of p_z , suggesting that the energy gain

is mainly in the gyro-rotation plane during the shock crossings. However, beyond ~ 0.06 s, the crests of p_x and p_z do not increase anymore, but the magnitude of p_z increases to the similar level of p_x and p_z . It is assumed that the energy homogenization among different directions are due to the pitch angle diffusion by magnetic turbulence. From the bottom panel of Figure 2, the particle gains energy more than 200 times of its initial energy. But beyond ~ 0.06 s, the particle energy keeps almost constant.

From the trajectories of test particle simulations, we calculate the energy spectra of accelerated particles for different simulation time. **In Figure 3 circles show the energy spectra of accelerated particles with different simulation time in the downstream of the shock. Note that we do not show the energy spectra with energies lower than the initial energy E_{in} , since in reality below E_{in} the background spectrum is dominant. Here we show spectra of the acceleration time of 10, 20, 55, ..., 495 ms. We can see that the energy spectrum hardens and extends to higher energies with increasing of time. The spectrum at $t = 495$ ms reaches as high as 100 MeV compared to ~ 10 MeV for the case of $t = 10$ ms. In addition, the spectra at lower energies show a power-law with a bend-over energy E_0 . As time increased the spectra with power-law do not change significantly with the bend-over energy increased.**

Furthermore, we fit the simulated data using a power law with an exponential tail from Equation (6) in log-log space, adopting the nonlinear least-squares fitting algorithm. The best-fit parameters, C , α , and E_0 are listed in Table 2. In Figure 3, we plot the fitted energy spectra with solid and dashed lines. The result provides a good fit to the simulated energy spectra. This indicates that in our simulations the spectra of the accelerated particles in the downstream exhibit a form of a power law with an exponential tail.

In addition, we present the energy spectra of $t = 25, 90, 225, 440$ ms in Figure 4. It is shown that the power law with an exponential tail form fits well to the simulated energy spectra. The oblique and vertical lines indicate the spectral index and bend-over energy. From this figure we can see that the bend-over energy, E_0 , increases from ~ 1.6 MeV to ~ 22 MeV within 500 ms. Moreover, in the same acceleration time range, generally, spectral index α increases from 0.85 to 0.96.

In Figure 5 we show the evolution of the power-law index, α , of the shock accelerated particle energy spectrum from simulations as shown in Figure 3 with time (open circles). The dashed line indicates

the theoretical index γ from Equation (5) by Decker and Vlahos (1986). It is shown that the power law index from simulations is always smaller than the theoretical results, but generally it increases with acceleration time. In addition, as the acceleration time becomes larger, the simulated power-index approaches the theoretical one more and more.

Figure 6 shows the time evolution of the bend-over energy, E_0 . Red diamonds show the results of bend-over energy from simulations E_0^{sim} . Solid and dotted lines indicate the results from theory Equation (16) with diffusion models NLGCE-F and QLT, $E_0^{\text{NLGCE-F}}$ and E_0^{QLT} , respectively. It can be seen that E_0^{sim} , $E_0^{\text{NLGCE-F}}$, and E_0^{QLT} all increase with time. In addition, $E_0^{\text{NLGCE-F}}$ is always about 5 times that of E_0^{QLT} . At short acceleration time, $t \sim 10$ ms, E_0^{sim} is about 6.5 times that of $E_0^{\text{NLGCE-F}}$, but E_0^{sim} increases slower than $E_0^{\text{NLGCE-F}}$ does, so at $t \gtrsim 100$ ms E_0^{sim} is similar to $E_0^{\text{NLGCE-F}}$. In conclusion, at any acceleration time, $E_0^{\text{NLGCE-F}}$ is more consistent with E_0^{sim} than E_0^{QLT} does. Additionally, at larger acceleration time, $E_0^{\text{NLGCE-F}}$ agrees well with E_0^{sim} .

5. SUMMARY AND CONCLUSIONS

The well-known hybrid code is an effective approach to study particle acceleration and shock evolution self-consistently. It is, however, of interest to study the shock acceleration of energetic particles with some pre-determined shock conditions, e.g., geometry, compression ratio, magnetic fields, shock speed, and magnetic turbulence models. In addition, since test-particle simulations require much less computational resources, it is possible for us to study particle acceleration with more statistics in larger computation space and time. In this paper, we focus on particle acceleration at the parallel shock with numerical calculations of the trajectories of test particles by solving the equation of motion in turbulent magnetic fields. We simplify the shock to be an infinitely thin plane, and assume static magnetic turbulence superimposed on the static background magnetic field.

Our simulations indicate that charged particles can be accelerated to high energies, and even the energy gains of some particles can reach a few hundreds of times of their initial energy within several hundred milliseconds. We find that the energy spectrum of the shock-accelerated particles from simulations shows **a power law with an exponential tail**. The spectral index of the lower energy range agrees well with the

theoretical power law index model by [Decker and Vlahos \(1986\)](#). It is also found that from simulations the bend-over energy increases with time.

Theoretically, using the mean acceleration time and the average momentum change during each cycle of particles crossing of the shock ([Drury 1983](#)), we get the energy E_{acc} of shock-accelerated particles as a function of time. In addition, we assume the bend-over energy is equal to E_{acc} since it is less possible for particles to be accelerated to energies higher than E_{acc} at any time. The theoretical bend-over energy depends on the diffusion model. We compare the bend-over energy from simulations with that from theory adopting either QLT or NLGCE-F for the diffusion model, and find that **the simulated bend-over energy has a good agreement with the bend-over energy model obtained with NLGCE-F**. This result implies that the method of our test-particle simulations for shock accelerations can indirectly demonstrate that the diffusion model NLGCE-F is more accurate than QLT ([Qin and Zhang 2014](#)).

Our results from both numerical simulations and theoretical models show that the **charged particles accelerated at the parallel shock could produce the energy spectrum of a power-law with an exponential tail**. In this work, because of the limit of computational resources, we do not simulate the shock acceleration for a very long time, so that we do not obtain a power-law spectrum of energetic particles with the bend-over energy as large as that observed in the solar wind. In the future, we plan to study shock acceleration with much longer time so that we might be able to obtain more realistic power-law spectrum of energetic particles.

This work was supported by the Strategic Priority Research Program of Chinese Academy of Sciences (Grant No. XDA17010301). The work was also supported, in part, under grants NNSFC 41874206 and NNSFC 41574172. The work was carried out at National Supercomputer Center in Tianjin, and the calculations were performed on TianHe-1 (A).

REFERENCES

- | | |
|---|---|
| Amato, E., & Blasi, P. 2005, MNRAS, 364, L76 | Bell, A. R. 1978, MNRAS, 182, 147 |
| Amato, E., & Blasi, P. 2006, MNRAS, 371, 1251 | Bell, A. R. 2004, MNRAS, 353, 550 |

- Bieber, J. W., Matthaeus, W. H., Shalchi, A. & Qin, G. 2004, *Geophys. Res. Lett.*, 31, L10805
- Decker, R. B. 1988, *SSRv*, 48, 195
- Decker, R. B., & Vlahos, L. 1986, *ApJ*, 306, 710
- Dosch, A., Adhikari, L., & Zank, G. P. 2013, 13th International Solar Wind Conference (Solar Wind 13), 1539, 155
- Drury, L. O'C. 1983, *Rep. Prog. Phys.*, 46, 973
- Ellison, D. C., Baring, M. G., & Jones, F. C. 1995, *ApJ*, 453, 873
- Ellison, D. C., & Ramaty, R. 1985, *ApJ*, 298, 400
- Fermi, E. 1949, *Phys. Rev.* 75, 1169
- Florinski, V., Zank, G. P., & le Roux, J. A. 2008, *Adv. Space Res.*, 41, 361
- Forman, M. A., & Webb, G. M. 1985, in *Collisionless Shocks in the Heliosphere: A Tutorial Review*, Geophysical Monograph, Vol. 34, ed. R. G. Stone & B. T. Tsurutani (Washington, DC: American Geophysical Union), 91
- Giacalone, J. 2004, *ApJ*, 609, 452
- Giacalone, J. 2005a, *ApJ*, 624, 765
- Giacalone, J. 2005b, *ApJL*, 628, L37
- Guo, F. & Giacalone, J. 2010, *ApJ*, 715, 406
- Guo, X. Y., Sironi, L., & Narayan, R. 2014, *ApJ*, 794, 153
- Jokipii, J. R. 1966, *ApJ*, 146, 480
- Jokipii, J. R. 1971, *Res. Geophys. Space Phys.*, 9, 27
- Jokipii, J. R. 1982, *ApJ*, 255, 716
- Jokipii, J. R., & Giacalone, J. 1996, *Spa. Sci. Rev.*, 78, 137
- Kirk, J. G., & Schneider, P. 1987, *ApJ*, 315, 425
- Kong, F. J., Qin G., & Zhang, L. H. 2017, *ApJ*, 845, 43
- Krülls, W. M., & Achterberg, A. 1994, *A&A*, 286, 314
- Lee, M. A., Shapiro, V. D., & Sagdeev, R. Z. 1996, *J. Geophys. Res.*, 101, 4777
- Li, G., Shalchi, A., Ao, X., Zank, G., & Verkhoglyadova, O. P. 2012, *J. Adv. Space Res.*, 49, 1067
- Mace, R. L., Matthaeus, W. H., & Bieber, J. W. 2000, *ApJ*, 538, 192
- Malkov, M. A., & Drury, L. O'C. 2001, *Rep. Prog. Phys.*, 64, 429
- Matthaeus, W. H., Goldstein, M. L., & Roberts, D. A. 1990, *J. Geophys. Res.*, 95, 20673
- Matthaeus, W. H., Qin, G., Bieber, J. W., & Zank, G. P. 2003, *ApJL*, 590, L53
- Osman, K. T., & Horbury, T. S. 2007, *ApJL*, 654, L103
- Parker, E. N. 1965, *Planet. Space Sci.*, 13, 9
- Qi, S.-Y., Qin, G., & Wang, Y. 2017, *Res. Astron. Astrophys.*, 17, 33
- Qin, G. 2002, PhD thesis, UNIVERSITY OF DELAWARE
- Qin, G. 2007, *ApJ*, 656, 217
- Qin, G., Kong, F. J., & Zhang, L. H. 2018, *ApJ*, 860, 3
- Qin, G., Matthaeus, W. H., & Bieber, J. W. 2002a, *Geophys. Res. Lett.*, 29, 1048
- Qin, G., Matthaeus, W. H., & Bieber, J. W. 2002b, *ApJ*, 578, L117
- Qin, G., Wang, Y., Zhang, M., & Dalla, S. 2013, *ApJ*, 766, 74
- Qin, G., & Zhang, L. H. 2014, *ApJ*, 787, 12
- Qin, G., Zhang, M., & Dwyer, J.R. 2006, *J. Geophys. Res.*, 111, A08101

- Qin, G., Zhang, M., Dwyer, J.R., & Rassoul, H. K. 2004, *ApJ*, 609, 1076
- Shapiro, V. D., & Üçer, D. 2003, *Planet. Space Sci.*, 51, 665
- Shen, Z. N., & Qin, G. 2018, *ApJ*, 854, 137
- Skilling, J. 1971, *ApJ*, 170, 265
- Sugiyama, T. 2011, *Phys. Plasmas*, 18, 022302
- Sun, P., Qin, G., & Wang, C. 2007, *Chin. J. Space Sci.*, 27, 441
- Virtanen, J. J. P., & Vainio, R. 2005, *ApJ*, 621, 313
- Wang, Y., Qin, G., & Zhang, M. 2012, *ApJ*, 752, 37
- Weygand, J. M., Matthaeus, W. H., Dasso, S., et al. 2009, *J. Geophys. Res.*, 114, A07213
- Weygand, J. M., Matthaeus, W. H., Dasso, S., & Kivelson, M. G. 2011, *J. Geophys. Res.*, 116, A08102
- Winske, D., & Omid, N. 1996, *J. Geophys. Res.*, 101, 17287
- Zank, G. P., Rice, W. K. M., & Wu, C. C. 2000, *J. Geophys. Res.*, 105, 25079
- Zuo, P., Zhang, M., Gamayunov, K., Rassoul, H. K., & Luo, X. 2011, *ApJ*, 738, 168
- Zuo, P., Zhang, M., & Rassoul, H. K. 2013, *ApJ*, 767, 6

Table 1. Values of ξ_i and κ_{Ri} from NLGCE-F and QLT

Theory	Parameter	Upstream	Downstream
NLGCE-F	ξ_i	1.60	1.51
	κ_{Ri} (m ² /s)	8.48×10^{12}	3.10×10^{12}
QLT	ξ_i	1.33	1.33
	κ_{Ri} (m ² /s)	1.26×10^{13}	6.32×10^{12}

Table 2. Fitted Parameters for Time-dependent Energy Spectra

t (ms)	$C(10^{-3})$	α	E_0 (MeV)
10	0.36	0.85	1.59
20	0.29	0.87	2.29
55	0.29	0.78	3.29
105	0.25	0.81	5.29
150	0.23	0.83	6.96
200	0.21	0.86	9.03
250	0.20	0.88	11.01
300	0.18	0.92	13.98
375	0.17	0.93	16.95
495	0.16	0.96	21.67

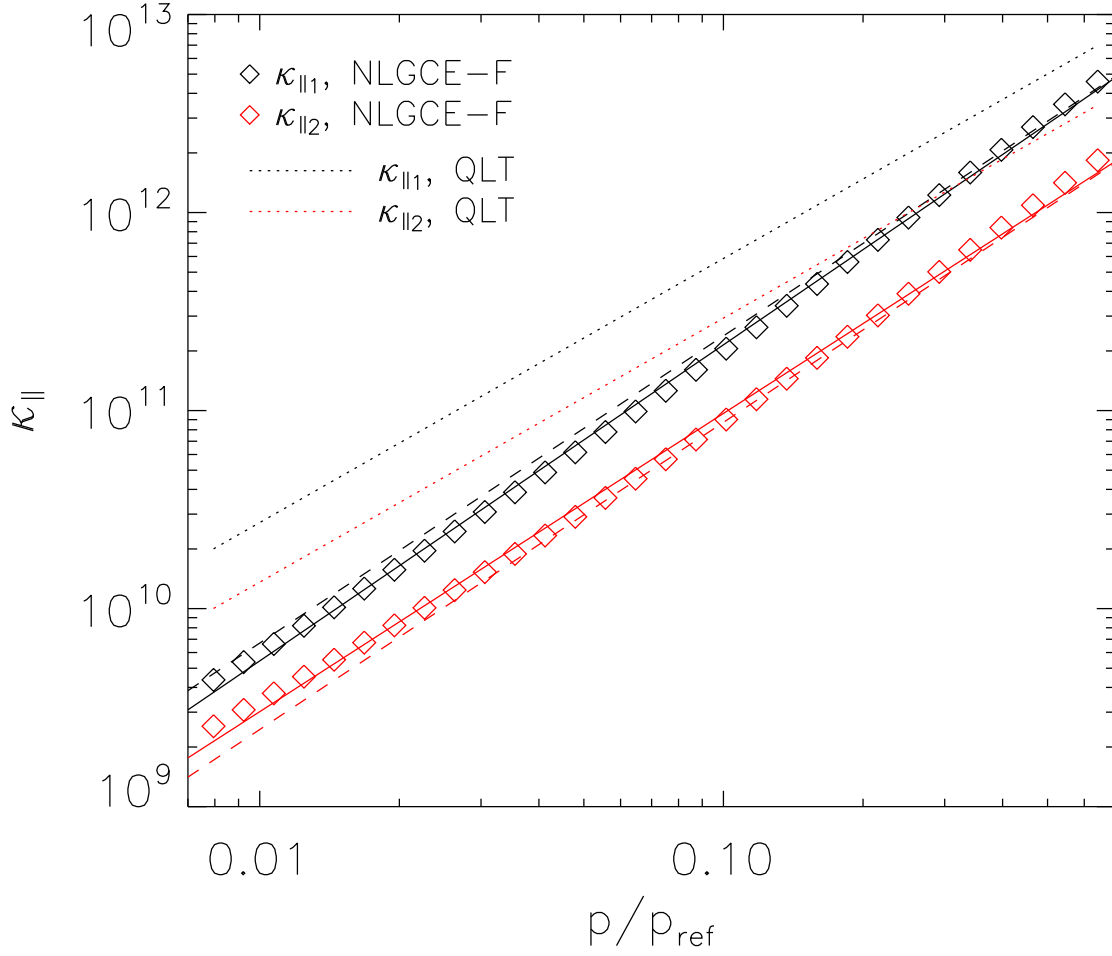


Figure 1. Parallel diffusion coefficients, $\kappa_{||1}$ and $\kappa_{||2}$, in the upstream (black) and downstream (red) of the shock, respectively, as a function of particle momentum p/p_{ref} , where p_{ref} is the momentum of a proton with rigidity $R = 1$ GV. The diamonds represent calculation results from NLGCE-F. The solid lines indicate the fitting of the NLGCE-F results using the power-law form in Equation (11) with power indices ξ_1 and ξ_2 in the upstream and downstream, respectively. To replace the power indices ξ_1 and ξ_2 with the average value, the solid lines are changed to the dashed lines. The dotted lines indicate the QLT results.

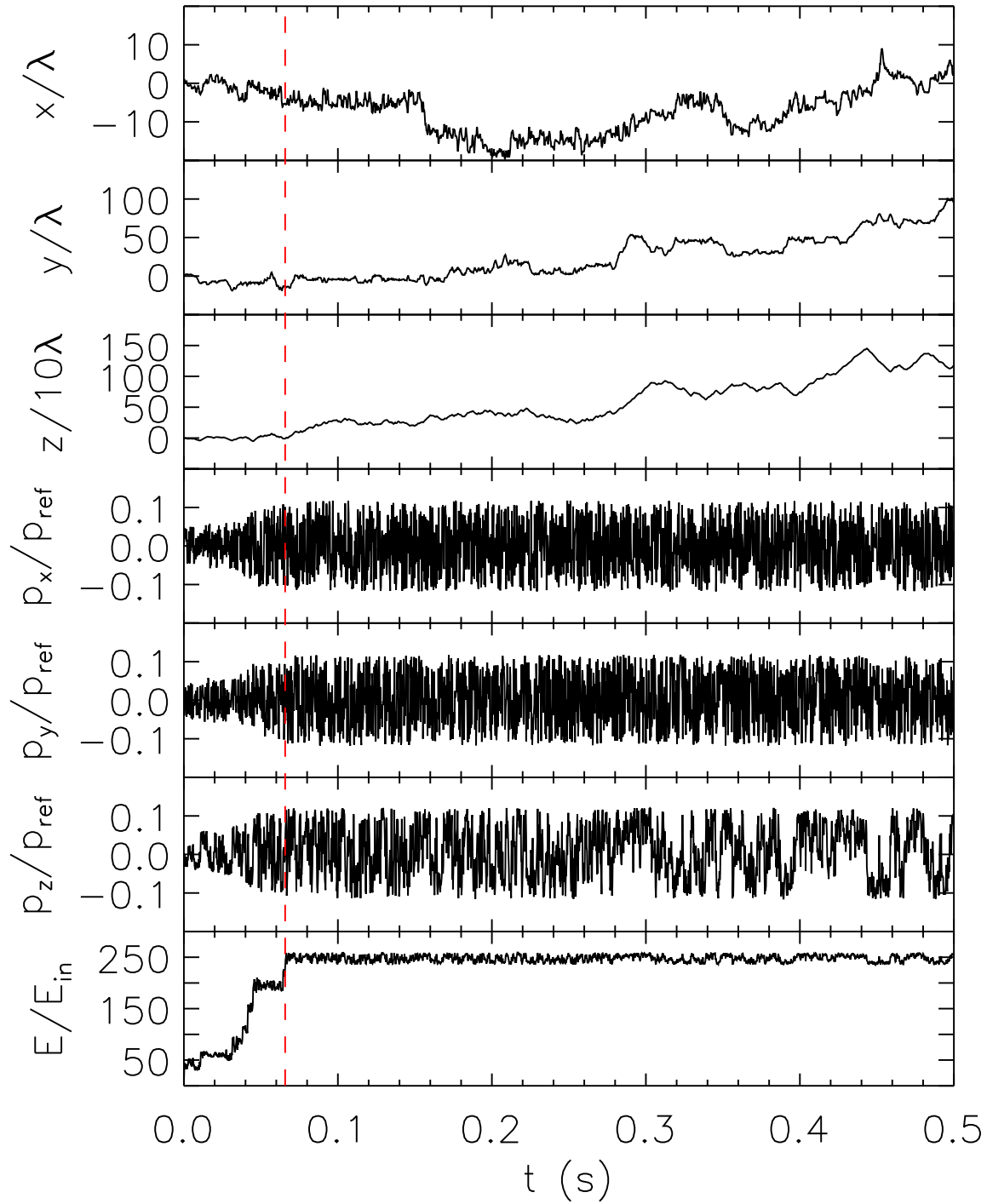


Figure 2. Trajectory of a test particle as a function of time. The top three panels show the particle position in the Cartesian coordinate system, the fourth to sixth panels show the particle momentum in each direction, and the bottom panel indicates the particle energy. The vertical red line indicates the time when the particle does not cross the shock again.

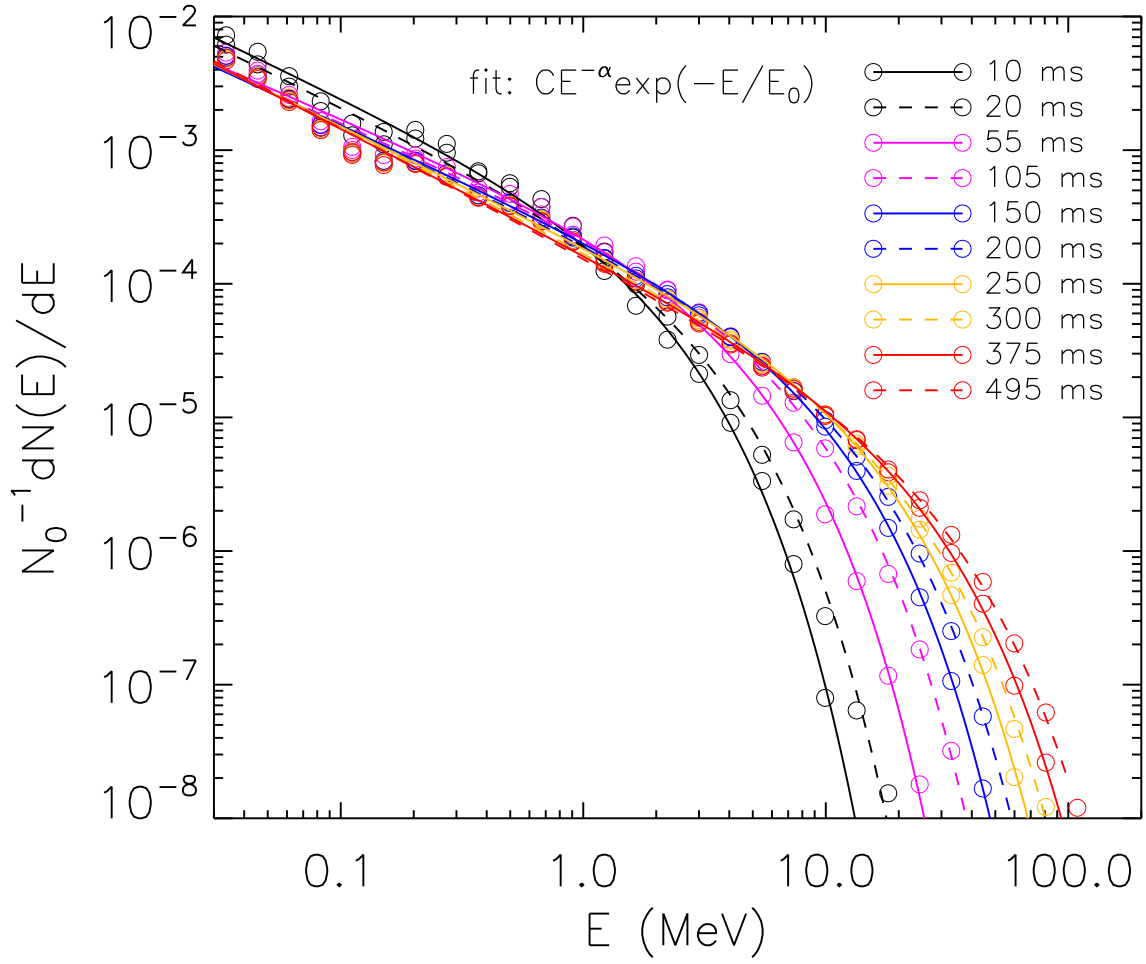


Figure 3. Downstream energy spectra of accelerated particles for different simulation times (circles). Solid and dashed lines indicate Fits to the simulated energy spectra using the function form in Equation 6, at various simulation times.

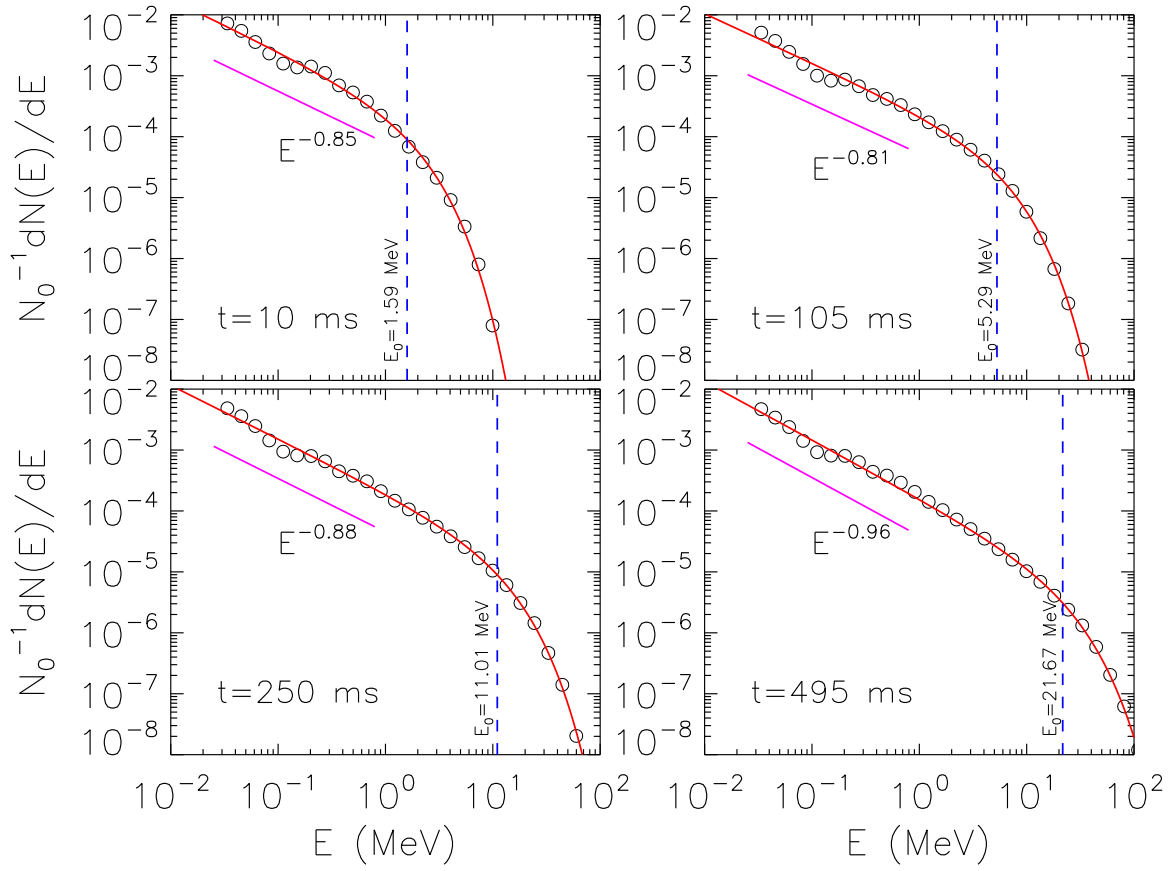


Figure 4. Fits to the simulated spectra (open circles) at $t = 10, 105, 250, 495$ ms are plotted in red curves. The blue vertical line and magenta oblique line in each panel denote the bend-over energy E_0 and the spectral index.

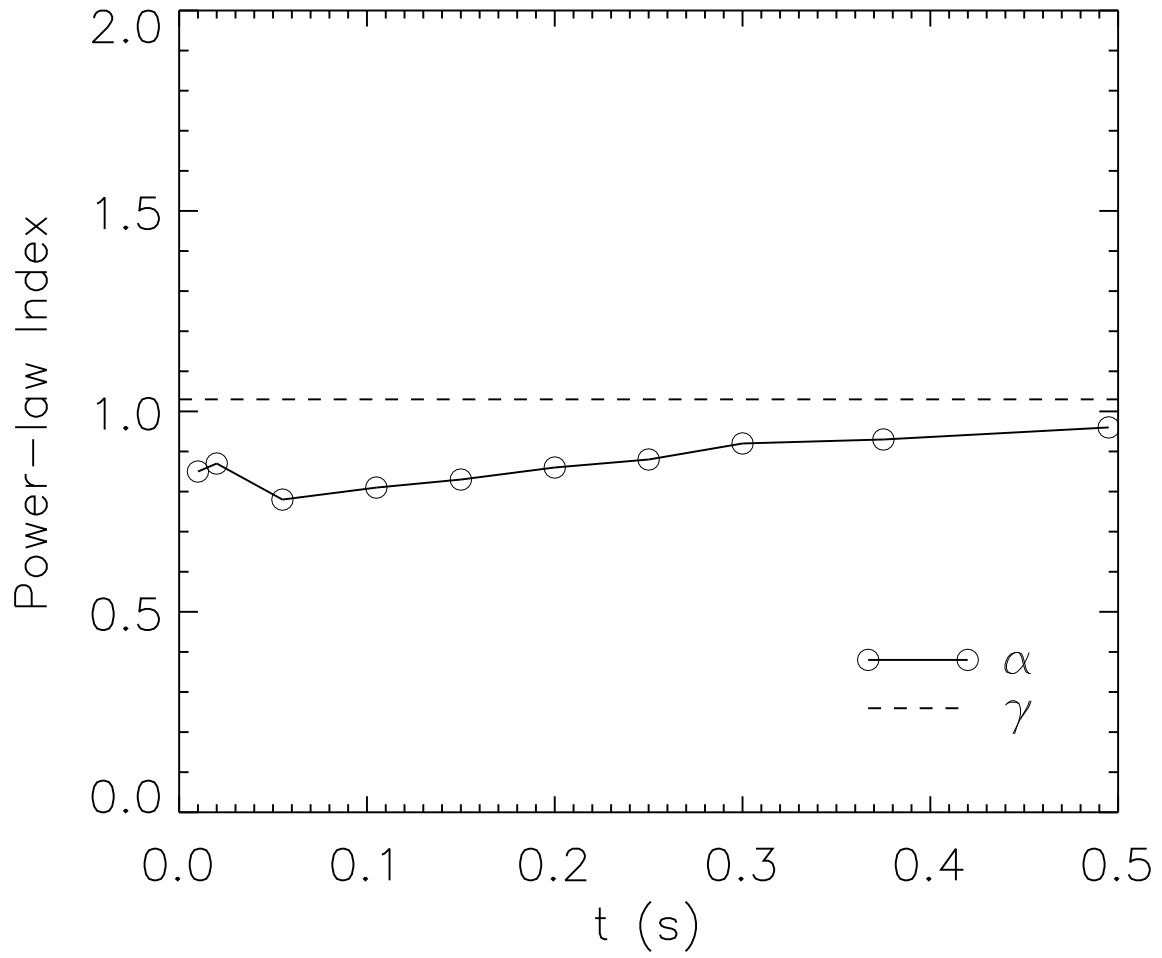


Figure 5. Spectral index of shock accelerated particles as a function of time. The circles indicate results from simulations, and the dashed line corresponds to DSA theory.

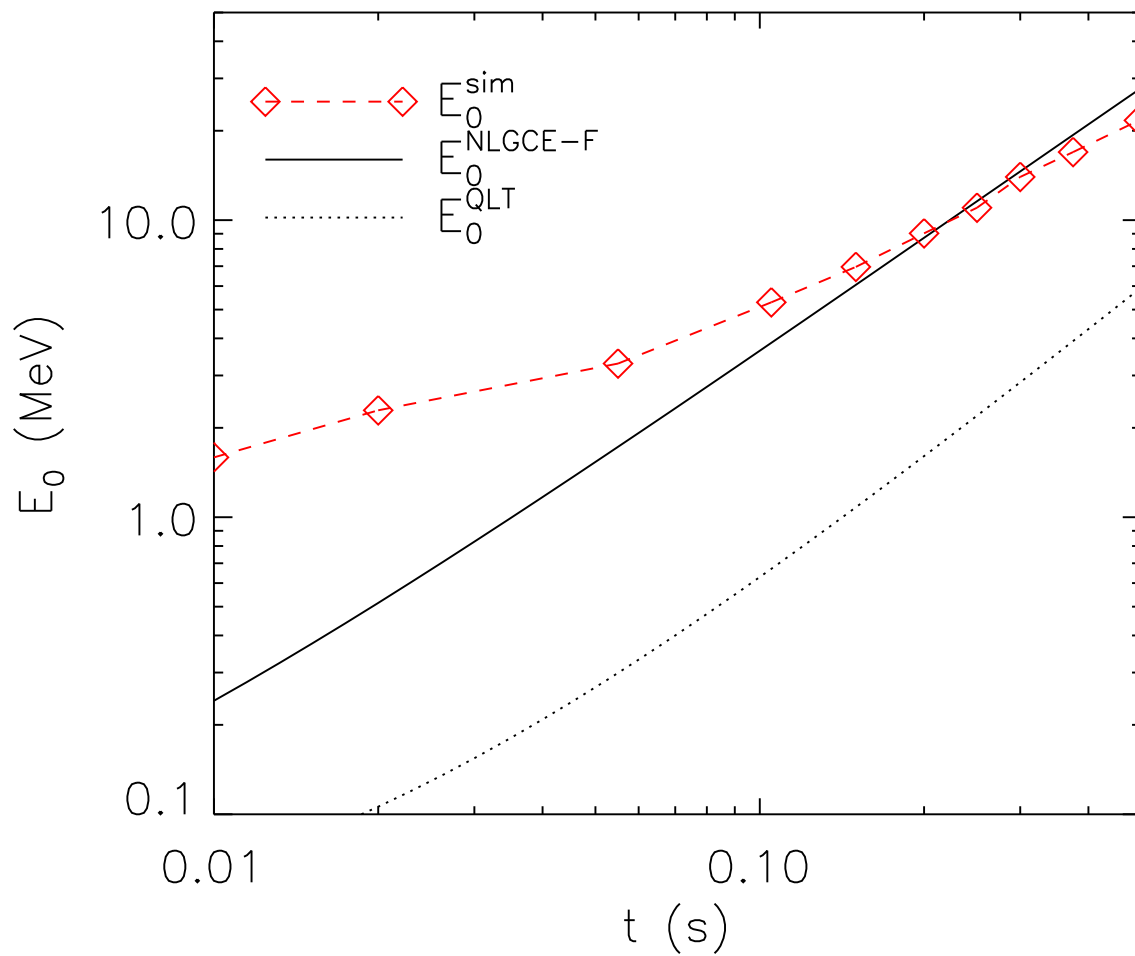


Figure 6. Bend-over energy, E_0 , as a function of time from simulations (diamonds), theory with NLGCE-F (solid line), and theory with QLT (dotted line).